







## Nature and impact of charge transfer to ground-state dications in atomic and molecular environments

C. Küstner-Wetekam <sup>1,\*</sup>, X. Q. Hu <sup>2,\*</sup>, L. Marder <sup>1</sup>, Ph. Schmidt,<sup>3</sup> C. Ozga,<sup>1</sup> Ch. Zindel,<sup>1</sup> H. Otto,<sup>1</sup> Y. G. Peng,<sup>2</sup> J. G. Wang,<sup>2</sup> C. Richter,<sup>4,5</sup> N. Sisourat,<sup>6</sup> U. Hergenhahn <sup>4,5</sup>, A. Knie,<sup>1</sup> A. Ehresmann <sup>1</sup>, Y. Wu,<sup>2,7,‡</sup> and A. Hans <sup>1,§</sup>

<sup>1</sup>*Institut für Physik und CINSaT, Universität Kassel, Heinrich-Plett-Straße 40, D-34132 Kassel, Germany*

<sup>2</sup>*The Key Laboratory of Computational Physics, Institute of Applied Physics and Computational Mathematics, Beijing 100088, China*

<sup>3</sup>*European XFEL GmbH, D-22869 Schenefeld, Germany*

<sup>4</sup>*Leibniz-Institut für Oberflächenmodifizierung (IOM), Permoserstraße 15, D-04318 Leipzig, Germany*

<sup>5</sup>*Fritz-Haber-Institut der Max-Planck-Gesellschaft, Faradayweg 4-6, D-14195 Berlin, Germany*

<sup>6</sup>*Laboratoire de Chimie Physique Matière et Rayonnement, UMR 7614, Sorbonne Université, CNRS, F-75005 Paris, France*

<sup>7</sup>*Center for Applied Physics and Technology, HEDPS, Peking University, Beijing 100871, China*



(Received 19 March 2021; accepted 21 September 2021; published 6 October 2021)

Charge transfer processes between weakly bound entities play an important role in various chemical and biological environments. In this combined experimental and theoretical work, we investigate the nature of charge-transfer processes in homogeneous atomic and heterogeneous atomic-molecular clusters. Our results reveal fundamentally different processes to be at play in pure argon clusters compared to mixed argon-nitrogen systems: We demonstrate that the former species decay via photon-mediated charge transfer while a nonradiative direct process is found dominant in the atomic-molecular cases. Our results are of general interest for studies on charge redistribution in more complex and biologically relevant samples where molecules are involved.

DOI: [10.1103/PhysRevA.104.042802](https://doi.org/10.1103/PhysRevA.104.042802)

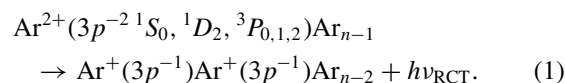
### I. INTRODUCTION

The decay of electronic vacancies is one of the most fundamental processes in atomic physics. Depending on the initially ionized state and the stored excess energy, an atomic ion may either decay radiatively via fluorescence, by autoionization, i.e., emission of an Auger electron, or cascades of these processes, finally reaching the ionic ground state. In molecules, the decay may additionally be accompanied by dissociation. This situation changes significantly, if the ion is in an environment. Here, additional interatomic (intermolecular) relaxation pathways are possible as part of the decay (cascade) [1–4]. Even the ground-state ion may decay further into an energetically preferred state of the whole system by charge transfer [5–8].

From prototypes to complex systems, such interatomic (intermolecular) charge and energy transfer processes are the decisive factors for the final charge distribution. Knowledge about the charge distribution is thus a critical ingredient for many models on photon-matter interaction, e.g., Coulomb imaging of large clusters and biomolecules. Also, the radiation damage to biological systems induced by ionizing radiation critically depends on the immediate relaxation of the initially ionized site. The investigation of prototypical atomic clusters gives insight into the fundamentals and nature of interatomic processes. To obtain a better understanding of

whether a certain process is biologically relevant, it is however necessary to increase the complexity of the considered system. It was observed recently, that further processes come into play if the two charges are located at a molecule in an environment, such as proton transfer in hydrogen bond dimers [9,10] and heavy  $N^+$  ion transfer in van der Waals  $N_2$ -Ar dimers [11]. In the present article, we address the charge dissipation from atomic dications in heterogeneous clusters, in which a rare-gas species is mixed with a molecule. We find that the molecular properties fundamentally change the nature of the charge transfer.

More specifically, we investigate the relaxation pathways of pure atomic argon and mixed argon-nitrogen clusters after  $2p$  photoionization of Ar. In the exemplary case of isolated Ar atoms, the energy stored is above the second ionization potential, which leads to relaxation by Auger decay, preferably to the dicationic  $Ar^{2+}(3p^{-2})$  ground state. In an atomic cluster it is energetically favorable if one electron of a neighboring neutral Ar atom is transferred to the dicationic  $Ar^{2+}$  and a photon is emitted via the so-called radiative charge-transfer (RCT) process [5,12,13]:



The energy of the emitted photon can be estimated from the potential energy curves of the dicationic states and the internuclear distance at which the RCT takes place. For Ar dimers, these energies are 6.6, 8.3, and 10.7 eV for different Auger final states [13].

By combining high-level *ab initio* calculations and electron-electron-photon coincidence spectroscopy

\*These authors contributed equally to this work.

†c.kuestner-wetekam@uni-kassel.de

‡wu\_yong@iapcm.ac.cn

§hans@physik.uni-kassel.de

measurements, we investigate the influence of increased complexity, introduced by embedding molecules into atomic clusters.

## II. THEORY

We calculated the one-site dicationic and two-site dicationic potential energy curves (PECs) of Ar-Ar and Ar-N<sub>2</sub> dimers. The replacement of Ar by N<sub>2</sub> is ideally suited to study the increase of complexity going along with the presence of molecules without changing the overall properties of the system too much, since Ar and N<sub>2</sub> have comparable ionization potentials. Our calculations and their impact on the nature of the charge transfer are supported by electron-electron-photon coincidence experiments on Ar clusters with different N<sub>2</sub> admixtures.

The PECs are computed using the multireference double-excited configuration-interaction method (MRDCI) [14,15] with molecular orbitals optimized by the complete active space self-consistent field method (CASSCF) [16,17], in which the orbital wave functions are expanded on augmented correlation-consistent polarized valence-only triple-zeta (aug-cc-pVTZ) basis sets. It should be noted that different active space orbitals are chosen for the calculations of N<sub>2</sub><sup>q+</sup> ( $q = 0, 1, 2$ ) and Ar<sub>2</sub><sup>2+</sup>. For the case of N<sub>2</sub><sup>q+</sup>, all valence orbitals of (2s2p) are included in the active space, but for the case of Ar<sub>2</sub><sup>2+</sup>, both the valence orbitals of (3s3p) and the Rydberg orbitals of (4s4p) are included. For the PECs of (N<sub>2</sub>Ar)<sup>2+</sup>, the calculations are performed using the nonexcited MRCI method. Based on their relative contributions in varying the CI energy, in total about 20 000 reference configurations are used to optimize the PECs of (N<sub>2</sub>Ar)<sup>2+</sup>, which contain the ground-state configuration and a large number of singly excited, doubly excited, triply excited, and quadruply excited configurations. Due to the noninclusion of higher excited configurations, the errors in the calculated energies are about 0.2 eV at a large internuclear distance of  $R_{N_2-Ar}$  for the PECs of (N<sub>2</sub>Ar)<sup>2+</sup>.

For the PECs of highly excited Ar<sup>+</sup>-N<sub>2</sub><sup>+\*</sup>, they are calculated by a Coulomb potential model. Due to the very similar ionization potentials of Ar and N<sub>2</sub>, the repulsive two-site dicationic curves Ar<sup>+</sup> + Ar<sup>+</sup> and Ar<sup>+</sup> + N<sub>2</sub><sup>+</sup> are almost identical (blue solid curves in Fig. 1). The same holds for the one-site dicationic curve of Ar<sup>2+</sup> with Ar or N<sub>2</sub> as the dimer partner (black solid curve). For the energetically lowest Ar<sup>2+</sup> configuration (<sup>3</sup>P<sub>0,1,2</sub>) in the Ar dimer, RCT happens at the equilibrium distance of the Ar<sup>2+</sup>-Ar PEC, releasing a photon of ~6 eV energy and two energetic Ar<sup>+</sup> ions. Note that the lowest excited state of Ar<sup>+\*</sup> + Ar<sup>+</sup> character is considerably higher in energy (green dashed curve) and does not interfere with the process. In strong contrast, the Ar<sup>+</sup> + N<sub>2</sub><sup>+</sup> system exhibits a manifold of states of Ar<sup>+</sup> + N<sub>2</sub><sup>+\*</sup> character, some of which (red curves) are crossing the Ar<sup>2+</sup>-N<sub>2</sub> curve. Since the Auger decay into the Ar<sup>2+</sup> state can be assumed to happen in the equilibrium geometry of the Ar-N<sub>2</sub> dimer (indicated by the black arrow), the system is expected to start at that Ar-N<sub>2</sub> distance on the Ar<sup>2+</sup>-N<sub>2</sub> PEC. Due to nuclear dynamics on its way towards the new equilibrium distance, it couples to the Ar<sup>+</sup> + N<sub>2</sub><sup>+\*</sup> states via nonradiative direct single charge transfer (SCT).

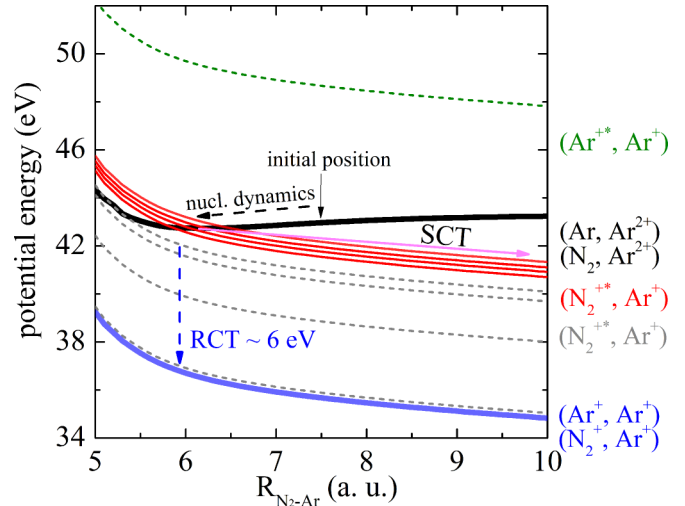


FIG. 1. Potential energy curves of one-site dicationic (Ar-Ar<sup>2+</sup>), (N<sub>2</sub>-Ar<sup>2+</sup>), and two-site dicationic (Ar<sup>+</sup> + Ar<sup>+</sup>) and (Ar<sup>+</sup> + N<sub>2</sub><sup>+</sup>) configurations.

## III. EXPERIMENT

The experiment was performed at the Helmholtz-Zentrum Berlin (BESSY II) using the synchrotron radiation of the U49-2 PGM-1 beamline. We ensured comparability with our previous work on pure Ar clusters [13] by using the identical experimental setup, target source, and spectrometer settings. The experimental setup for electron-photon coincidence spectroscopy combines a magnetic bottle-type time-of-flight electron spectrometer with photon detection by a mirror assembly and a single-photon detector [18,19]. The photon detector, consisting of a CsTe photocathode, a microchannel-plate (MCP) stack, and a hexagonal anode, is sensitive for single photons in the energy range between 4.0 and 10.4 eV [20]. The cluster jet was produced by supersonic expansion of gaseous Ar-N<sub>2</sub> mixtures through an 80- $\mu$ m conical copper nozzle (30° opening angle), cryogenically cooled using a liquid N<sub>2</sub> cryostat. The resulting target jet passed a 1-mm skimmer before crossing the linearly polarized, monochromatic synchrotron radiation. For proper energy resolution in the Auger electron spectrum, a -192 V retardation potential was applied to the electron drift tube. For further details, see Ref. [13]. For a systematic investigation of different amounts of N<sub>2</sub> in Ar clusters, identical measurements were performed for gas mixtures containing from 0% to 66% N<sub>2</sub>. We emphasize that this mixing ratio does not represent the final composition of the clusters, which we cannot determine precisely in the present experiment. The target jet also contains a residual amount of uncondensed atoms and molecules. Although the exact composition is unknown, a comparison to literature assures that mixed clusters form under these conditions [21,22].

## IV. RESULTS AND DISCUSSION

To investigate the predicted quenching of RCT due to SCT in a heterogeneous cluster, Ar clusters with a N<sub>2</sub> admixture were prepared using 0%, 33%, 50%, 60%, and 66% N<sub>2</sub> in the initial gas mixture. The Auger spectra of the partially

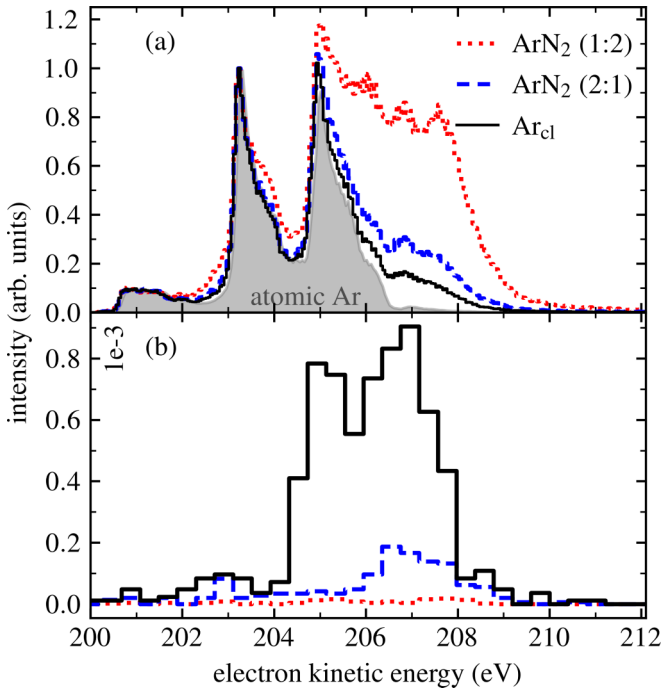


FIG. 2. Electron spectra after  $2p$  ionization of Ar clusters excited with a photon energy of 449 eV. (a) Auger spectra of partially condensed cluster jets at 80 K nozzle temperature for pure Ar (black solid), 33% (blue dashed), and 66% (red dashed-dotted)  $N_2$  admixtures, obtained from electron-electron coincidences with  $2p_{3/2}$  photoelectrons. An atomic reference spectrum is shown as the gray shaded area. (b) The corresponding spectra obtained from electron-electron-photon coincidences, normalized to the cluster signal in (a) after subtraction of the atomic reference.

condensed cluster jet obtained after  $2p$  photoionization of Ar are shown in Fig. 2.

Figure 2(a) compares the Auger spectra for pure Ar clusters to mixed clusters formed after an admixture of 33% and 66%  $N_2$ , obtained from electron-electron (EE) coincidence spectra of the  $LMM$  Auger electron and the  $2p_{3/2}$  photoelectron. These spectra show two characteristic peaks at 203.3 and 204.9 eV electron kinetic energy, which can be attributed to Auger decay into the atomic  $^1D_2$  and  $^3P_{0,1,2}$  states within the remaining free Ar atoms in the jet [12]. For comparison, a pure atomic Auger spectrum taken with identical spectrometer settings is shown (gray shaded area). The broad feature at higher kinetic energies corresponds to Auger decay in Ar clusters [5,23–25]. Since the different initial mixtures lead to different total amounts of Ar atoms and clusters in the target jet, we normalized each spectrum to the atomic Auger signal ( $^1D_2$ ) of the atomic reference spectrum. With increasing  $N_2$  content, the spectrum shows more prominent cluster characteristics. We conclude that due to the higher total pressure in the gas reservoir, larger Ar clusters are formed by the addition of  $N_2$ , which is in qualitative agreement with commonly used cluster size scaling laws [21,22].

In order to isolate the sole contributions of the clusters, we employ electron-electron-photon (EEP) coincidences. The corresponding spectra are shown in Fig. 2(b). Each spectrum has been normalized to the integrated cluster signal intensity

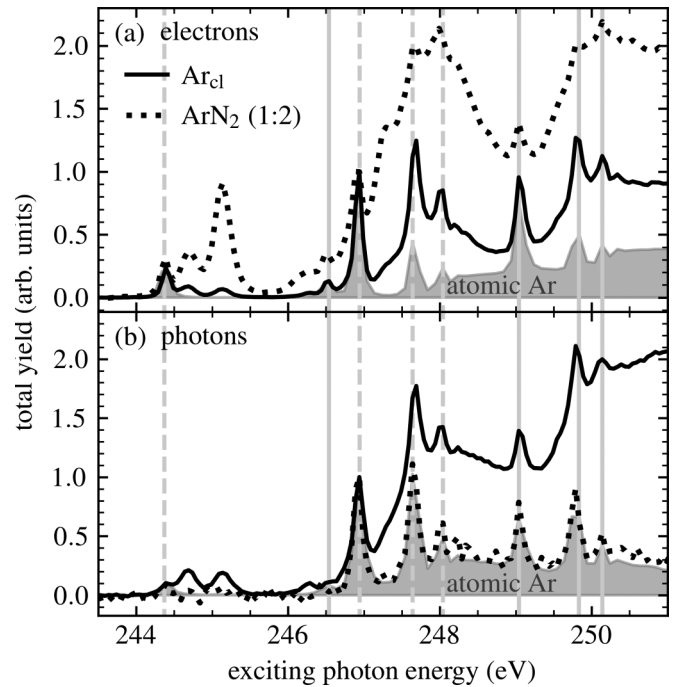


FIG. 3. (a) Total electron yields across the Ar  $2p$  edge, for atomic Ar (dashed), a partially condensed Ar cluster jet with a nozzle temperature of  $T = 105$  K (solid), and a partially condensed Ar- $N_2$  (66%  $N_2$ ) cluster jet with a nozzle temperature of  $T = 80$  K (dotted). (b) Corresponding total UV photon yields. The gray vertical lines indicate the  $2p_{1/2}-nl$  (solid) and  $2p_{3/2}-nl$  (dashed) atomic Rydberg series.

of the electron-electron coincidences in Fig. 2(a) after subtraction of the atomic reference spectrum. The spectra in Fig. 2(b) thus represent the number of electron-electron-photon coincidences per cluster-specific electron-electron coincidence. The spectrum of pure Ar clusters in Fig. 2(b) shows the expected shape, which we observed in our recent work [13]. An addition of 33%  $N_2$ , however, results in a drastic drop in intensity and for 66%  $N_2$  the signal has vanished below a statistically significant level. This is a clear indication that in mixed Ar- $N_2$  clusters a new decay channel opens, which quenches the RCT. We attribute this to the aforementioned SCT process predicted by our calculations. Importantly, the Auger spectra in Fig. 2(a) confirm that the admixture of  $N_2$  does not hinder the formation of Ar clusters but supports the condensation process. To consolidate these observations, we scanned the exciting-photon energy stepwise from 243 to 253 eV (in steps of 50 meV) and recorded the total electron yields [Fig. 3(a)] and photon yields [Fig. 3(b)] for atomic Ar (dashed line), pure Ar clusters (solid line), and mixed Ar- $N_2$  (66%  $N_2$ ) clusters (dotted line). This particular energy range was chosen as it covers the  $2p-nl$  Rydberg series and the  $2p_{3/2}$  and  $2p_{1/2}$  ionization thresholds of atomic Ar [26] and Ar clusters [27]. In both panels of Fig. 3, the data are normalized to coincide in intensity at the atomic  $2p_{3/2}-3d$  resonance peak at about 246.9 eV for a better comparison.

The energetically lowest peak at 244.37 eV originates from the atomic  $3p_{3/2}-4s$  resonance. It results in electron emission due to resonant Auger decay, but also leads to some photons

mainly from the spectator Auger final states of  $\text{Ar}^{+*}(2p^4nl)$  character [28,29], which decay further by fluorescence. In Fig. 3(a), additional features in the total electron yield are observed when changing from atomic Ar to clusters. Particularly, we notice the appearance of two additional peaks at the high-energy side of the atomic  $2p_{3/2}$ - $4s$  resonance, which are attributed to the surface and the bulk  $2p_{3/2}$ - $4s$  cluster resonances, respectively [30]. Starting from 247 eV, there is a rather unstructured increase in electron yield, originating from broad and overlapping  $2p$ - $nl$  Rydberg series in clusters [31]. The addition of  $\text{N}_2$  to the Ar clusters further promotes the cluster-specific features in the total yield. The bulk  $2p_{3/2}$ - $4s$  resonance took over compared to its surface counterpart, and the atomic resonances just remain as weak peaks on the broad cluster signal, which is a strong indication for the creation of large Ar- $\text{N}_2$  clusters. There are two different contributions to this effect. First, the higher expansion pressure supports the formation of larger clusters, and second, the mixed Ar- $\text{N}_2$  clusters are known to form core-shell structures with Ar being the core and  $\text{N}_2$  at the surface [21].

Information on the nature of the charge transfer from the dicationic  $\text{Ar}^{2+}$  is contained in the corresponding total photon yields shown in Fig. 3(b). Similar to the total electron yield, for atomic Ar the  $2p$ - $nl$  Rydberg series can clearly be identified, but with different intensities due to varying branching ratios of participator and spectator Auger decay. As expected, when changing to Ar clusters, the  $2p_{3/2}$ - $4s$  surface and bulk cluster resonances appear as well. Additionally, there is a significant increase in the total photon yield in two steps, namely at the ionization potentials of  $2p_{3/2}$  (247.4 eV) and  $2p_{1/2}$  (249.5 eV) in clusters [32]. This increase can be attributed to the RCT process, as  $2p$  ionization starts to efficiently populate RCT initial states. Upon the addition of  $\text{N}_2$ , the curve resembles the one of atomic Ar within the experimental statistics. We therefore conclude that, while indeed large Ar- $\text{N}_2$  clusters are produced, a competing relaxation process with higher efficiency quenches the RCT signal completely.

We determine the decrease in RCT signal for different Ar- $\text{N}_2$  mixing ratios. For the smallest chosen  $\text{N}_2$  admixture of 33%, the ratio already drops to 19% and decreases further with higher  $\text{N}_2$  admixtures to only 2% at 66%  $\text{N}_2$ , which is below the systematic uncertainty of the experiment. We quantify the decrease in RCT signal compared to the overall cluster signal by integrating the EEP coincidence counts for different Ar- $\text{N}_2$  mixing ratios, normalized to the intensity of

TABLE I. Initial mixing ratio (given as Ar and  $\text{N}_2$  flow), resulting pressure in the gas reservoir, and ratio of EEP coincidence counts normalized to EE coincidence cluster counts. The ratio is set to be 1 for the pure Ar case. The given uncertainties are purely statistical uncertainties emerging from the calculation.

Ar (sccm)	$\text{N}_2$ (sccm)	$\text{N}_2$ (%)	$p$ (mbar)	EEP/EE
10	0	0	200	$1.00 \pm 0.05$
10	5	33	300	$0.19 \pm 0.02$
10	10	50	390	$0.08 \pm 0.01$
10	15	60	490	$0.09 \pm 0.01$
10	20	66	560	$0.020 \pm 0.003$

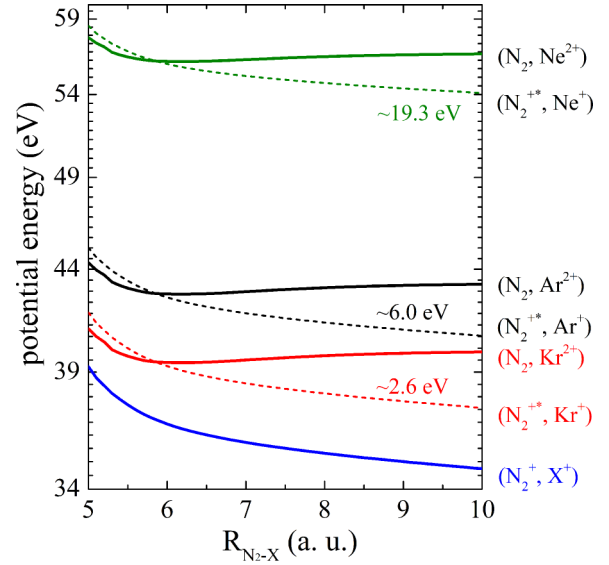


FIG. 4. Potential energy curves of  $(\text{N}_2\text{X})^{2+}$  ( $X = \text{Ne}, \text{Ar}, \text{Kr}$ ), in which the solid lines represent the potential energy curves of ground states  $\text{N}_2^+\text{X}^{2+}$  and  $\text{N}_2^+\text{X}^{2+}$ , and the dashed lines are the ones of the first excited states of  $\text{N}_2^+\text{X}^+$ . Note that 2.6, 6.0, and 19.3 eV are the relative excitation energies of  $\text{N}_2^{+*}\text{Kr}^+$ ,  $\text{N}_2^{+*}\text{Ar}^+$ , and  $\text{N}_2^{+*}\text{Ne}^+$ , respectively.

the cluster signal in EE coincidences after the subtraction of the atomic reference. The resulting ratios for all initial mixing conditions are summarized in Table I, in which the ratio is set to be 1 for the pure Ar case. In Table I, only the statistical uncertainties are given, emerging from the calculation of the ratio. In the present case, it is difficult to reasonably estimate the systematic uncertainty of the experiment, since the final composition of the clusters cannot be determined in this experiment.

The observed nonradiative charge transfer is expected to be a general mechanism for ions in molecular environments. As a natural extension of  $(\text{Ar}_2)^{2+}$  and  $(\text{N}_2\text{Ar})^{2+}$  systems, the potential energy curves of  $(\text{N}_2\text{Ne})^{2+}$  and  $(\text{N}_2\text{Kr})^{2+}$  are computed with the same method and shown in Fig. 4. Similar to the  $\text{N}_2\text{Ar}$  case it is found that a manifold of crossings exists between the ground  $\text{N}_2^+\text{X}^{2+}$  and excited states  $\text{N}_2^{+*}\text{X}^+$  ( $X = \text{Kr}, \text{Ar}, \text{Ne}$ ), which quench the RCT processes efficiently. Moreover, with increasing ionization energies for  $\text{Kr}^+$ ,  $\text{Ar}^+$  and  $\text{Ne}^+$ , the energy differences between the ground states of  $(\text{N}_2^{+*}, \text{X}^+)$  and  $(\text{N}_2^+, \text{X}^+)$  ( $X = \text{Kr}, \text{Ar}, \text{Ne}$ ) become larger and the corresponding  $\text{N}_2^{+*}$  become more energetic and dissociative.

## V. CONCLUSION

Summarizing, we investigated the nature and impact of charge-transfer processes to atomic dicationic ground-state ions in an environment. When changing the system from homogeneous atomic Ar clusters to heterogeneous atomic-molecular Ar- $\text{N}_2$  clusters, radiative charge transfer is efficiently quenched by nonradiative direct charge transfer. The change originates from a manifold of excited  $\text{N}_2^{+*}$  states which intersect with the one-site dicationic states. Our results suggest that radiative charge transfer is generally quenched

in molecular systems and may stimulate further experimental and theoretical efforts to understand the detailed role and nature of charge-transfer processes.

#### ACKNOWLEDGMENTS

We thank L. S. Cederbaum, K. Gokhberg, and N. Kryzhevoi for valuable discussions. We thank HZB for

beamtime allocation and the BESSY II staff for assistance. This work was funded by the Deutsche Forschungsgemeinschaft (DFG) (Project No. 328961117 – SFB 1319 ELCH and Research Unit FOR 1789) and by the Federal Ministry of Education and Research of Germany (BMBF) in the framework of project 05K19RK2. Y.W. and X.Q.H. are supported by the National Natural Science Foundation of China under Grant No. 11934004.

- 
- [1] L. S. Cederbaum, J. Zobeley, and F. Tarantelli, *Phys. Rev. Lett.* **79**, 4778 (1997).
- [2] U. Hergenhahn, *J. Electron Spectrosc. Relat. Phenom.* **184**, 78 (2011).
- [3] T. Jahnke, *J. Phys. B: At. Mol. Opt. Phys.* **48**, 082001 (2015).
- [4] T. Jahnke, U. Hergenhahn, B. Winter, R. Dörner, U. Frühling, P. V. Demekhin, K. Gokhberg, L. S. Cederbaum, A. Ehresmann, A. Knie, and A. Dreuw, *Chem. Rev.* **120**, 11295 (2020).
- [5] N. Saito, Y. Morishita, I. H. Suzuki, S. D. Stoychev, A. I. Kuleff, L. S. Cederbaum, X.-J. Liu, H. Fukuzawa, G. Prümper, and K. Ueda, *Chem. Phys. Lett.* **441**, 16 (2007).
- [6] D. You, H. Fukuzawa, Y. Sakakibara, T. Takanashi, Y. Ito, G. G. Maliyar, K. Motomura, K. Nagaya, T. Nishiyama, K. Asa, Y. Sato, N. Saito, M. Oura, M. Schöffler, G. Kastirke, U. Hergenhahn, V. Stumpf, K. Gokhberg, A. I. Kuleff, L. S. Cederbaum *et al.*, *Nat. Commun.* **8**, 14277 (2017).
- [7] A. Hans, V. Stumpf, X. Holzapfel, F. Wiegand, P. Schmidt, C. Ozga, P. Reiß, L. B. Ltaief, C. Küstner-Wetekam, T. Jahnke, A. Ehresmann, P. V. Demekhin, K. Gokhberg, and A. Knie, *New J. Phys.* **20**, 012001 (2018).
- [8] A. Hans, C. Ozga, P. Schmidt, G. Hartmann, A. Nehls, P. Wenzel, C. Richter, C. Lant, X. Holzapfel, J. H. Viehmann, U. Hergenhahn, A. Ehresmann, and A. Knie, *Rev. Sci. Instrum.* **90**, 093104 (2019).
- [9] C. Richter, D. Hollas, C.-M. Saak, M. Förstel, T. Miteva, M. Mucke, O. Björneholm, N. Sisourat, P. Slavíček, and U. Hergenhahn, *Nat. Commun.* **9**, 4988 (2018).
- [10] S. Xu, D. Guo, X. Ma, X. Zhu, W. Feng, S. Yan, D. Zhao, Y. Gao, S. Zhang, X. Ren, Y. Zhao, Z. Xu, A. Dorn, L. S. Cederbaum, and N. V. Kryzhevoi, *Angew. Chem. Int. Ed. Engl.* **57**, 17023 (2018).
- [11] X. Zhu, X. Hu, S. Yan, Y. Peng, W. Feng, D. Guo, Y. Gao, S. Zhang, A. Cassimi, J. Xu, D. Zhao, D. Dong, B. Hai, Y. Wu, J. Wang, and X. Ma, *Nat. Commun.* **11**, 2987 (2020).
- [12] L. O. Werme, T. Bergmark, and K. Siegbahn, *Phys. Scr.* **8**, 149 (1973).
- [13] A. Hans, C. Küstner-Wetekam, P. Schmidt, C. Ozga, X. Holzapfel, H. Otto, C. Zindel, C. Richter, L. S. Cederbaum, A. Ehresmann, U. Hergenhahn, N. V. Kryzhevoi, and A. Knie, *Phys. Rev. Res.* **2**, 012022(R) (2020).
- [14] R. J. Buenker and R. A. Phillips, *J. Mol. Struct.: THEOCHEM* **123**, 291 (1985).
- [15] S. Krebs and R. J. Buenker, *J. Chem. Phys.* **103**, 5613 (1995).
- [16] H.-J. Werner, P. J. Knowles, G. Knizia, F. R. Manby, M. Schütz, P. Celani, W. Györffy, D. Kats, T. Korona, R. Lindh, A. Mitrushenkov, G. Rauhut, K. R. Shamasundar, T. B. Adler, R. D. Amos, S. J. Bennie, A. Bernhardsson, A. Berning, D. L. Cooper, M. J. O. Deegan *et al.*, MOLPRO: A package of *ab initio* programs, version 2010.1 (2010), <http://www.molpro.net>.
- [17] P. J. Knowles and H.-J. Werner, *Chem. Phys. Lett.* **115**, 259 (1985).
- [18] M. Mucke, M. Förstel, T. Lischke, T. Arion, A. M. Bradshaw, and U. Hergenhahn, *Rev. Sci. Instrum.* **83**, 063106 (2012).
- [19] A. Hans, T. Miteva, X. Holzapfel, C. Ozga, P. Schmidt, H. Otto, G. Hartmann, C. Richter, N. Sisourat, A. Ehresmann, K. Gokhberg, U. Hergenhahn, and A. Knie, *Phys. Rev. Lett.* **123**, 213001 (2019).
- [20] A. Hans, P. Schmidt, C. Ozga, G. Hartmann, X. Holzapfel, A. Ehresmann, and A. Knie, *Materials* **11**, 869 (2018).
- [21] M. Nagasaka, E. Serdaroglu, R. Flesch, E. Rühl, and N. Kosugi, *J. Chem. Phys.* **137**, 214305 (2012).
- [22] O. P. Konotop, S. I. Kovalenko, O. G. Danylchenko, and V. N. Samovarov, *J. Cluster Sci.* **26**, 863 (2015).
- [23] M. Lundwall, M. Tchapyguine, G. Öhrwall, A. Lindblad, S. Peredkov, T. Rander, S. Svensson, and O. Björneholm, *Surf. Sci.* **594**, 12 (2005).
- [24] M. Lundwall, A. Lindblad, H. Bergersen, T. Rander, G. Öhrwall, M. Tchapyguine, S. Peredkov, S. Svensson, and O. Björneholm, *J. Phys. B: At. Mol. Opt. Phys.* **39**, 3321 (2006).
- [25] M. Lundwall, A. Lindblad, G. Öhrwall, S. Svensson, and O. Björneholm, *Phys. Rev. A* **78**, 065201 (2008).
- [26] O.-P. Sairanen, A. Kivimäki, E. Nömmiste, H. Aksela, and S. Aksela, *Phys. Rev. A* **54**, 2834 (1996).
- [27] A. Kivimäki, S. L. Sorensen, M. Tchapyguine, M. Gisselbrecht, R. R. T. Marinho, R. Feifel, G. Öhrwall, S. Svensson, and O. Björneholm, *Phys. Rev. A* **71**, 033204 (2005).
- [28] H. Aksela, S. Aksela, H. Pulkkinen, G. M. Bancroft, and K. H. Tan, *Phys. Rev. A* **37**, 1798 (1988).
- [29] Y. Lu, W. C. Stolte, and J. A. R. Samson, *Phys. Rev. A* **58**, 2828 (1998).
- [30] E. Rühl, C. Heinzl, A. P. Hitchcock, and H. Baumgärtel, *J. Chem. Phys.* **98**, 2653 (1993).
- [31] I. L. Bradeanu, R. Flesch, M. Meyer, H.-W. Jochims, and E. Rühl, *Eur. Phys. J. D* **36**, 173 (2005).
- [32] M. Tchapyguine, R. Feifel, R. Marinho, M. Gisselbrecht, S. Sorensen, A. Naves de Brito, N. Mårtensson, S. Svensson, and O. Björneholm, *Chem. Phys.* **289**, 3 (2003).